Nuclear Engineering and Design 460 (2026) 115284

Contents lists available at ScienceDirect

Nuclear Engineering and Design

journal homepage: www.elsevier.com/locate/nucengdes

Evaluation of kinetic parameters and nuclear data-induced uncertainty analysis of β_{eff} for the DNRR research reactor using Monte Carlo method

Duc-Tu Dau [a,*], Nhi-Dien Nguyen [a], Giang T.T. Phan [b], Huu-Tiep Nguyen [c], Peng Hong Liem [d,e], Hoai-Nam Tran [f,*]

[a] Dalat Nuclear Research Institute, Vietnam Atomic Energy Institute, 01 Nguyen Tu Luc, Lamvien-Dalat, Lamdong 670000, Viet Nam
[b] Faculty of Electrical Engineering Technology, Industrial University of Ho Chi Minh City, Ho Chi Minh City 700000, Viet Nam
[c] Department of Quantum and Nuclear Engineering, Sejong University, 209, Neungdong-ro, Gwangjin-gu, Seoul 05006, Republic of Korea
[d] Tokyo City University, Graduate School of Engineering, Cooperative Major in Nuclear Energy, 1-28-1, Tamazutsumi, Setagaya, Tokyo, Japan
[e] Nippon Advanced Information Service, (NAIS Co., Inc.), Scientific Computational Division, 416 Muramatsu, Tokaimura, Ibaraki, Japan
[f] Phenikaa Institute for Advanced Study, Phenikaa University, Hanoi 12116, Viet Nam

ARTICLE INFO

Keywords:
Kinetic parameters
Sensitivity analysis
Data-induced uncertainty
DNRR
MCNP6.3

ABSTRACT

This study evaluates the kinetic parameters, including the effective delayed neutron fraction (β_{eff}), neutron generation time (Λ), and prompt neutron lifetime (l_p), for the Dalat Nuclear Research Reactor (DNRR) with low enriched uranium fuel. Additionally, the nuclear data-induced uncertainty of β_{eff} was quantified. High fidelity simulations were performed using the MCNP6.3 code in conjunction with multiple latest evaluated nuclear data libraries, including ENDF/B-VIII.0, ENDF/B-VIII.1, JEFF-3.3, JENDL-5, and CENDL-3.2. The kinetic parameters (β_{eff}, Λ, l_p) were evaluated using the adjoint weighted method, and the prompt k-ratio method was applied to provide an independent comparison of β_{eff}. Depending on the data library, the calculated values for β_{eff}, Λ, and l_p ranged from 731 to 769 pcm, 80.31 to 80.91 μs, and 80.45 to 81.38 μs, respectively. For the baseline ENDF/B-VIII.0 library, the adjoint weighted calculations yielded the values of 739 pcm for β_{eff}, 80.31 μs for Λ, and 80.45 μs for l_p. Sensitivity and uncertainty analysis revealed that the aggregate β_{eff} uncertainty is primarily driven by the elastic scattering cross sections of Al-27, B-10, Be-9, and H-1, with Al-27 contributing significantly to the total uncertainty budget. These results provide a quantitative basis for the DNRR's kinetics analysis and underscore the necessity of employing comprehensive covariance data for reactor safety and licensing assessments.

1. Introduction

Kinetic parameters, specifically the effective delayed neutron fraction (β_{eff}), mean neutron generation time (Λ), and prompt neutron lifetime (l_p), are fundamental to the safety assessments and transient kinetics analyses of nuclear reactors (Khan et al., 2013; Nagaya, 2015; Arkani et al., 2016; Dau et al., 2025b,c; OECD, 2017). Among these parameters, β_{eff} is of particular importance in reactor kinetics and reactivity control, as it defines the reactivity unit "dollar", corresponding to the onset of prompt criticality. The delayed neutrons originate from the β^- decay of specific fission products, commonly categorized into six precursor groups based on their half lives and characterized by group constant quantities such as fractional yields (β_i) and decay constants (λ_i) (Nagaya, 2015; Akyurek et al., 2021; Dau et al., 2025b,c). The Λ is the mean time interval between the emission of a prompt neutron and the subsequent absorption event that leads to a fission reaction. The l_p refers to the average duration from the emission of a prompt neutron to its eventual absorption, either through fission, capture, or escape from the reactor core (Pinem et al., 2024; Hanson and Diamond, 2012; Dau et al., 2025b,c). The accuracy of reactor kinetic simulations strongly depends on the quality of the underlying nuclear data.

Significant research has been devoted to determining these parameters across various reactor types using Monte Carlo simulations (Bretscher, 1997; Romero-Barrientos et al., 2022; Hanson et al., 2006; Meulekamp and van der Marck, 2006; Hosseini et al., 2010; Pinem et al., 2024). Recently, sensitivity and uncertainty (S/U) analyses have emerged as a critical framework for quantifying how uncertainties in nuclear data, such as reaction cross sections and fission yields, propagate through complex simulations. Notable S/U investigations have been conducted for several research reactors, including the TRIGA Mark II and the RSG-GAS multipurpose reactor, utilizing codes like SUSD3D and MCNP (Kodeli, 2013; Mweetwa et al., 2018; Makhloul

* Corresponding authors.
E-mail addresses: tudd.re@dnri.vn (D.-T. Dau), nam.tranhoai@phenikaa-uni.edu.vn (H.-N. Tran).

https://doi.org/10.1016/j.nucengdes.2026.115284
Received 21 January 2026; Received in revised form 18 October 2026; Accepted 19 October 2026
Available online 30 October 2026
0029-5493/© 2026 Elsevier B.V. All rights are reserved, including those for text and data mining, AI training, and similar technologies.

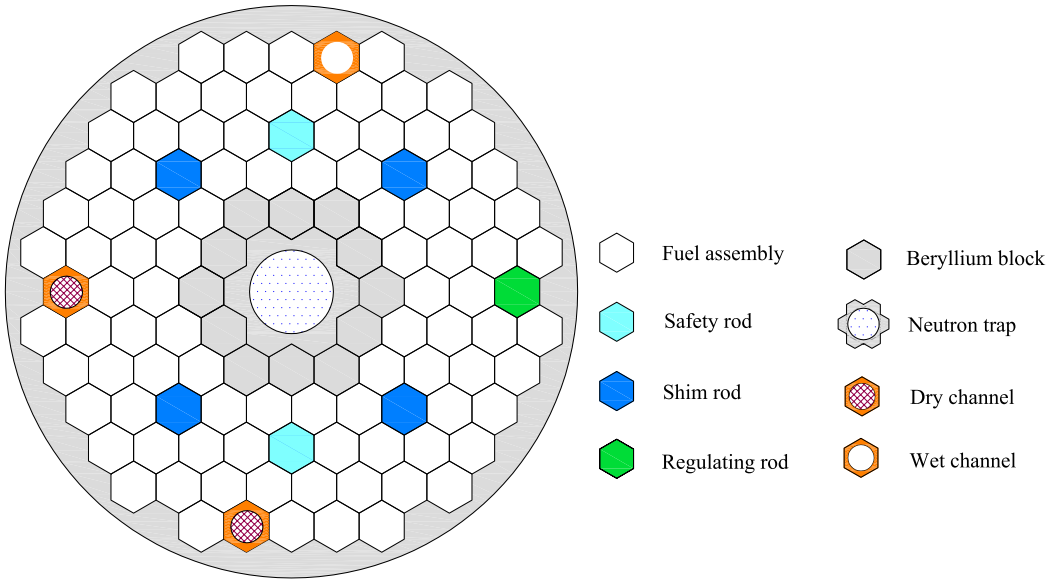


Fig. 1. Configuration of the DNRR consisting of 92 LEU fuel bundles.

et al., 2022; Liem et al., 2019; Chu et al., 2024; Dau et al., 2025a). These studies underscore that even minor discrepancies in evaluated covariance data across different libraries (e.g., ENDF/B, JENDL, JEFF) can lead to substantial variations in the predicted uncertainty of kinetic characteristics. In the context of kinetic parameters, uncertainties predominantly stem from nuclear data, namely, reaction cross sections, prompt and delayed fission neutron yields, delayed neutron emission probabilities, and the group-wise delayed neutron fractions (β_i). These input uncertainties are propagated through reactor simulations in conjunction with evaluated covariance data. Hence, uncertainty analysis plays an important role in quantifying the impact of nuclear data uncertainties on reactor parameter calculations, identifying the dominant contributors to calculation uncertainties, and supporting reactor core design, licensing, and safety analyses.

The Dalat Nuclear Research Reactor (DNRR) is a 500-kW pool type reactor which, since 2011, has utilized Low Enriched Uranium (LEU) fuel with a U-235 enrichment of 19.75 wt% (Nguyen, 2003; Nguyen et al., 2014; Dau et al., 2025a,b,c). The current core configuration consists of 92 LEU fuel assemblies, comprising 80 fresh and 12 partially depleted bundles (Nguyen et al., 2012; Dau et al., 2025a,b,c). To ensure operational efficiency and safety, a diverse suite of deterministic and Monte Carlo based computational tools has been deployed for neutronics analysis, safety assessment, and fuel management. These include the WIMSD/CITATION system (Phan et al., 2017), the SRAC code (Do et al., 2019), MCNP5/6.2 (Do et al., 2019; Chu et al., 2024), Serpent, and the PARCS code (Tran et al., 2021). While extensive research has characterized the steady state properties of the DNRR (Phan et al., 2017; Chu et al., 2024; Tran et al., 2021; Dau et al., 2025a), studies on its kinetic parameters have remained limited. A rigorous evaluation of these parameters is indispensable for reactor kinetic analysis, safety margin quantification, and transient response prediction. However, comprehensive sensitivity and uncertainty (S/U) analyses for the DNRR's LEU core configuration have not yet been performed. In addition, the influence of nuclear data uncertainties on the calculated β_{eff} remains unquantified.

The present study aims to evaluate the kinetic parameters of the DNRR LEU core and perform comprehensive S/U analyses for β_{eff}. High fidelity simulations were executed based on a fully heterogeneous DNRR core configuration using the MCNP6.3 code and the latest evaluated nuclear data libraries. Specifically, the adjoint weighted method was used to evaluate the kinetic parameters, while the prompt k-ratio method was independently applied to estimate β_{eff} and its corresponding sensitivity coefficients for comparison. Furthermore, this investigation propagates uncertainties from new data libraries, including ENDF/B-VIII.1 and JENDL-5, to identify the dominant nuclear data components, such as specific isotope cross sections and reaction channels, that contribute significantly to the total uncertainty of the calculated β_{eff}. The results are expected to refine the predictive fidelity of reactor kinetics modeling and provide quantitative information for the transient safety assessment and licensing updates of the DNRR.

Table 1
Specifications of the DNRR core with LEU fuel.

Specification	Description
Reactor type	Pool type
Nominal thermal power	500 kW
Moderator and Coolant	Light water
Cooling mechanism	Natural convection
Reflector	Graphite, Beryllium and water
Active core height	60 cm
Fuel type	VVR-M2 type
LEU fuel	UO_2-Al alloy
^{235}U enrichment	19.75 wt%
Fuel cladding	Aluminum alloy SAV-1
Number of control rods	7 (2 safety rods, 4 shim rods, 1 regulating rod)
Neutron measuring channels	6 (3 fission chambers, 3 ionization chambers)
Vertical channels	4 (1 neutron trap, 2 dry channels, 1 wet channel)
Horizontal channels	4 (1 tangential channel, 3 radial channels)

2. The DNRR and calculation model

2.1. The DNRR with LEU fuel

The DNRR core features a cylindrical geometry with a height of 60 cm and an equivalent diameter of 44.2 cm. It is composed of 121 hexagonal lattice positions to accommodate fuel bundles, control rods, irradiation facilities, and beryllium reflector blocks. The analyzed configuration consists of 92 LEU fuel bundles and 12 beryllium blocks. Key geometric and operational characteristics of the DNRR are summarized in Table 1 and Fig. 1 (Nguyen et al., 2012; Dau et al., 2025a).

The LEU fuel assembly of the Russian VVR-M2 design comprises three concentric annular fuel tubes, a top header, and a bottom tail. The outermost tube is hexagonal, with a flat to flat width of 32 mm, while the inner two fuel tubes are circular with outer diameters of 22 mm and 11 mm, respectively. All three tubes are of 3 layer construction,

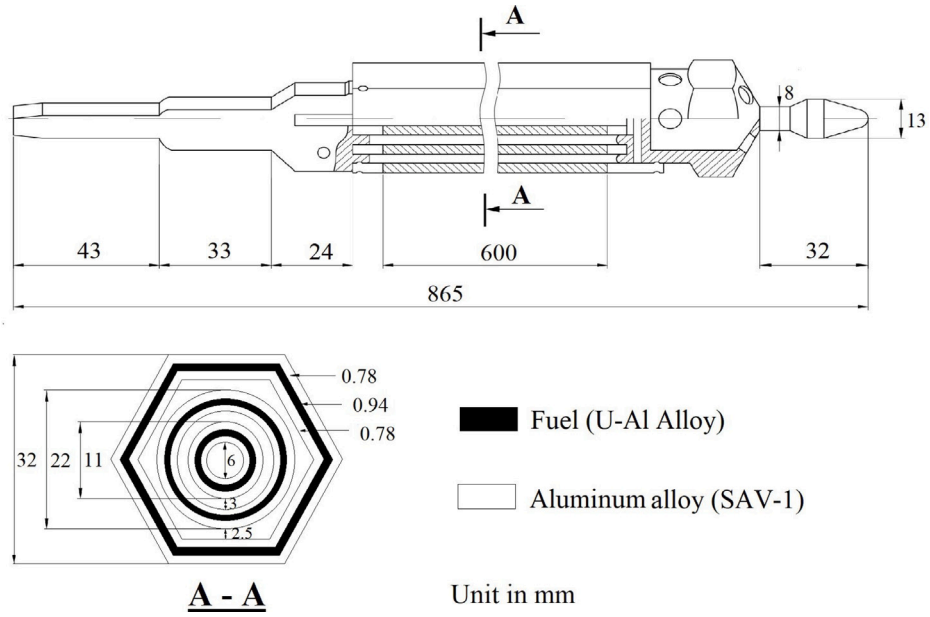


Fig. 2. Cross sectional view of the VVR-M2 type LEU fuel bundle.

Table 2
Design parameters of the VVR-M2 LEU fuel bundle.

Parameter	Value
Number of fuel tubes	3
Hexagonal tube	1
Cylindrical tube	2
Length of fuel bundle (mm)	
Total length	865
Fuel length	600
Fuel and cladding	
Cladding material	Aluminum alloy SAV-1
Fuel meat thickness (mm)	0.94
Cladding thickness (mm)	0.78
Fuel material	UO_2-Al alloy
Total U-235 mass (g)	49.7
U-235 enrichment (wt%)	19.75

consisting of a central fuel meat region with a thickness of 0.94 mm, clad on both sides with aluminum layers of 0.78 mm thickness. The annular gaps between tubes are approximately 2.5 to 3.0 mm, providing channels for coolant flow. The total length of a fuel bundle is 865 mm, including a 600 mm fueled region and aluminum sections. The fuel meat comprises uranium dioxide and aluminum (UO_2-Al), with an average content of 49.7 grams of U-235 per bundle. The structural and dimensional specifications of the LEU fuel bundle are illustrated in Fig. 2 and Table 2 (Nguyen, 2003; Nguyen et al., 2012, 2014; Dau et al., 2025a).

The control rod system comprises one automatic regulating rod (AR), four shim rods (ShRs), and two safety rods (SRs), each with an active absorber length of 65 cm to ensure complete coverage of the active core. The AR rod is fabricated from stainless steel, whereas the ShRs and SRs are made of boron carbide. Dry and wet irradiation channels are enclosed within aluminum tubes of 0.5 mm wall thickness. Centrally located within the core is a neutron trap composed of a 6.5 cm diameter water cylinder, 60 cm in length, surrounded symmetrically by twelve beryllium blocks, which adopt the same external geometry as the fuel assemblies. Surrounding the active core is a beryllium reflector, which in turn is enclosed by a 30.5 cm thick graphite reflector, providing additional neutron reflection (Nguyen et al., 2012; Dau et al., 2025a).

2.2. Calculation model

The MCNP6.3 neutron transport code (Kulesza et al., 2022) was utilized to model the complex core geometry of the DNRR. The DNRR computational model was developed based on the model presented in a previous study (Dau et al., 2025a). It explicitly represents the detailed structural configurations of the VVR-M2 fuel assemblies, beryllium rods, horizontal beam tubes, central neutron trap, radial beryllium and graphite reflectors, and the thermalizing column. The vertical and horizontal cross sectional views of the developed MCNP6.3 model are illustrated in Fig. 3. The model extends from the active core to the reactor tank, which is represented by an equivalent diameter of 198 cm and a height of 184.5 cm. The MCNP6.3 simulations were performed using 1000 active cycles and 100 initial inactive cycles to ensure convergence of the fission source distribution. Each cycle tracked 10^6 neutron histories, resulting in a low statistical uncertainty for k_{eff} within 3 pcm, as shown in Table 3.

Calculations were performed based on a representative experimental critical configuration of the DNRR LEU core, where the safety rods (SRs) were completely withdrawn, and the control rod positions were set at 430 mm for the shim rods (ShRs) and 390 mm for the automatic regulating rod (AR) (Dau et al., 2025a).

3. Kinetic parameters and uncertainty

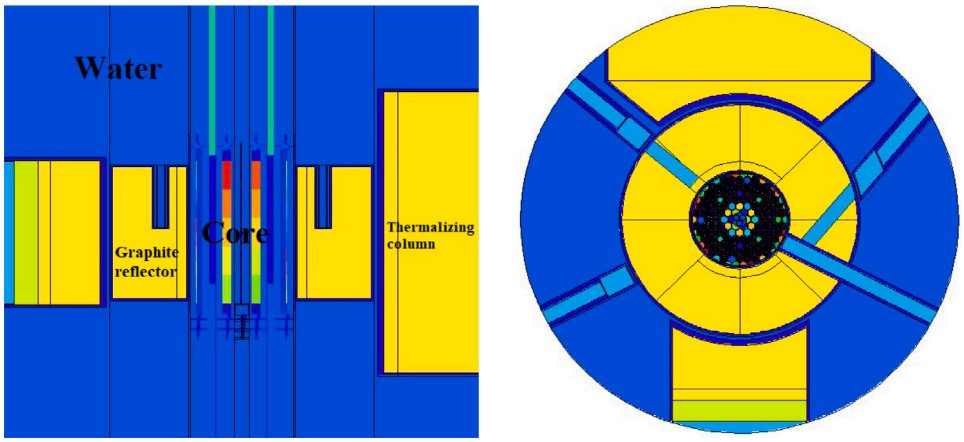
3.1. Effective kinetic parameters

The adjoint weighted method is formulated within the classical framework established by Keepin (1965), in which the effective delayed neutron fraction (β_{eff}) is defined as the ratio of the adjoint weighted delayed neutron production rate to the adjoint weighted total neutron production rate, as expressed in Eq. (1) (Talamo and Gohar, 2010; Meulekamp and van der Marck, 2006; Zhong et al., 2013; Kodeli, 2013; Kiedrowski and Brown, 2013; Romero-Barrientos et al., 2022; Pinem et al., 2024):

$$\beta_{\text{eff}} = \frac{\int \phi^+(\vec{r}, E', \Omega')\chi_d(E')\nu_d(E)\Sigma_f(\vec{r}, E)\phi(\vec{r}, E, \Omega)\, d\vec{r}\, dE'\, d\Omega'\, dE\, d\Omega}{\int \phi^+(\vec{r}, E', \Omega')\chi(E')\nu(E)\Sigma_f(\vec{r}, E)\phi(\vec{r}, E, \Omega)\, d\vec{r}\, dE'\, d\Omega'\, dE\, d\Omega}, \quad (1)$$

Table 3
Calculated criticality and kinetic parameters for the DNRR LEU core with various nuclear data libraries.

Calculation/Method	Parameters	ENDF/B-VIII.0	ENDF/B-VIII.1	JEFF-3.3	JENDL-5	CENDL-3.2
Criticality calculation	k_{eff}	1.00167 ± 0.00003	1.00285 ± 0.00003	1.00188 ± 0.00003	1.00321 ± 0.00003	1.00588 ± 0.00003
	$k_{\text{eff},p}$	0.99431 ± 0.00003	0.99550 ± 0.00003	0.99418 ± 0.00003	0.99584 ± 0.00003	0.99853 ± 0.00003
Adjoint-weighted method	β_{eff} (pcm)	739 ± 3	732 ± 3	756 ± 3	732 ± 3	734 ± 3
	Λ (μs)	80.31 ± 0.07	80.51 ± 0.07	80.44 ± 0.07	80.61 ± 0.07	80.91 ± 0.07
	l_p (μs)	80.45 ± 0.07	80.74 ± 0.07	80.59 ± 0.07	80.87 ± 0.07	81.38 ± 0.07
Prompt k-ratio method	β_{eff} (pcm)	735 ± 4	733 ± 4	769 ± 4	735 ± 4	731 ± 4



(a) Vertical cross-section (b) Horizontal cross-section

Fig. 3. Core model of the DNRR with LEU fuel.

By exploiting the linearity of the integral operators, Eq. (1) can be simplified as follows (Meulekamp and van der Marck, 2006):

$$\beta_{\text{eff}} = \frac{\langle \chi_d \nu_d \rangle}{\langle \chi \nu \rangle} = 1 - \frac{\langle \chi \nu - \chi_d \nu_d \rangle}{\langle \chi \nu \rangle} = 1 - \frac{\langle \chi \nu_p - (\chi_d - \chi)\nu_d \rangle}{\langle \chi \nu \rangle} \approx 1 - \frac{\langle \chi_p \nu_p \rangle}{\langle \chi \nu \rangle}, \tag{2}$$

where $\nu_d = \nu - \nu_p$, ν_p denotes the prompt neutron yield per fission, $\langle \cdot \rangle$ represents the integration over space and energy. The approximation on the right hand side of Eq. (2) is justified by the following arguments: (a) the term $(\chi_d - \chi)\nu_d$ is at least two orders of magnitude smaller than that associated with $\chi\nu_p$, because ν_d is approximately two orders of magnitude smaller than ν_p; and (b) the total fission neutron spectrum (χ) is nearly identical to the prompt fission neutron spectrum (χ_p) (Hendricks et al., 2006).

Following the derivation by Bretscher (1997), the β_{eff} is approximated using the prompt k-ratio method as:

$$\frac{\langle \chi_p \nu_p \rangle}{\langle \chi \nu \rangle} = \frac{k_{\text{eff},p}}{k_{\text{eff}}} \rightarrow \beta_{\text{eff}} \approx 1 - \frac{k_{\text{eff},p}}{k_{\text{eff}}}, \tag{3}$$

where k_{eff} and $k_{\text{eff},p}$ are the eigenvalues for total neutrons and for prompt neutrons only, respectively.

The neutron generation time, Λ, is defined as the average time between neutron birth and the absorption inducing fission. In reactor kinetics theory, this parameter is formally expressed using the forward and adjoint neutron fluxes as follows (Romero-Barrientos et al., 2022):

$$\Lambda = \frac{\int \phi^+(\vec{r}, \Omega, E) \frac{1}{v(E)} \phi(\vec{r}, \Omega, E) d\vec{r} d\Omega dE}{\int \phi^+(\vec{r}, \Omega, E) \chi(E) v(E) \Sigma_f(\vec{r}, E) \phi(\vec{r}, \Omega, E) dE d\Omega d\vec{r}}, \tag{4}$$

where $v(E)$ is the neutron speed. Correspondingly, the prompt neutron lifetime, l_p is calculated as (Hanson et al., 2006; Romero-Barrientos et al., 2022):

$$l_p = \Lambda \cdot k_{\text{eff}}. \tag{5}$$

3.2. Sensitivity and uncertainty analyses of β_{eff}

Sensitivity and uncertainty analyses enable identification of the main input data that influence reactor parameters and provide a quantitative assessment of modeling uncertainties. A comprehensive understanding of fundamental reactor parameters and reliable characterization of their associated uncertainties are crucial for reactor design (Kodeli, 2013). In this context, sensitivity analysis serves as an effective tool for identifying the specific nuclear data components that exert the most influence on β_{eff}. Since energy dependent neutron reaction cross sections constitute the primary inputs in neutronic simulations, the nuclear data induced uncertainty of the calculated β_{eff} can be rigorously quantified. This is achieved by propagating the corresponding sensitivity coefficients alongside nuclear data covariance matrices utilizing the conventional "sandwich rule" formulation.

For β_{eff} evaluation, the sensitivity estimation incorporates Bretscher's prompt k-ratio method (Bretscher, 1997) and the Adjoint Sensitivity Analysis Procedure (ASAP) (Cacuci et al., 2005). This approach enables a first order perturbation based evaluation of the relative contributions from various nuclear reactions. The sensitivity coefficient of β_{eff} with respect to a specific parameter α, denoted as $S_\alpha^{\beta_{\text{eff}}}$, is formally defined as follows (Kiedrowski, 2014; Kodeli, 2013):

$$S_\alpha^{\beta_{\text{eff}}} = \frac{\alpha}{\beta_{\text{eff}}} \frac{\partial \beta_{\text{eff}}}{\partial \alpha}. \tag{6}$$

By substituting Eq. (3) into Eq. (6), the sensitivity coefficient is expressed as:

$$\begin{aligned} S_\alpha^{\beta_{\text{eff}}} &= \frac{\alpha}{\beta_{\text{eff}}} \left(\frac{k_{\text{eff},p} \partial k_{\text{eff}}}{k_{\text{eff}}^2 \partial \alpha} - \frac{\partial k_{\text{eff},p}}{k_{\text{eff}} \partial \alpha} \right) \\ &= \frac{k_{\text{eff},p}}{k_{\text{eff}} - k_{\text{eff},p}} \left(\frac{\alpha \partial k_{\text{eff}}}{k_{\text{eff}} \partial \alpha} - \frac{\alpha \partial k_{\text{eff},p}}{k_{\text{eff},p} \partial \alpha} \right) \\ &= \frac{k_{\text{eff},p}}{k_{\text{eff}} - k_{\text{eff},p}} \left(S_\alpha^{k_{\text{eff}}} - S_\alpha^{k_{\text{eff},p}} \right), \end{aligned} \tag{7}$$

or

$$S_{\alpha}^{\beta_{\text{eff}}} = \frac{(1-\beta_{\text{eff}})}{\beta_{\text{eff}}}(S_{\alpha}^{k_{\text{eff}}} - S_{\alpha}^{k_{\text{eff},p}}), \tag{8}$$

where $S_{\alpha}^{k_{\text{eff}}}$ and $S_{\alpha}^{k_{\text{eff},p}}$ are the sensitivities of the k_{eff} and $k_{\text{eff},p}$, respectively, obtained from the standard linear perturbation theory (Kulesza et al., 2022). The uncertainty ($\sigma_{S_{\alpha}^{\beta_{\text{eff}}}}$) of the sensitivity coefficient of β_{eff} was estimated as:

$$\sigma_{S_{\alpha}^{\beta_{\text{eff}}}} = \sqrt{\frac{\left(S_{\alpha}^{k_{\text{eff}}} - S_{\alpha}^{k_{\text{eff},p}}\right)^2}{\beta_{\text{eff}}^4}\sigma_{\beta_{\text{eff}}}^2 + \left(\frac{1-\beta_{\text{eff}}}{\beta_{\text{eff}}}\right)^2\left(\sigma_{S_{\alpha}^{k_{\text{eff}}}}^2 + \sigma_{S_{\alpha}^{k_{\text{eff},p}}}^2\right)}, \tag{9}$$

where $\sigma_{S_{\alpha}^{k_{\text{eff}}}}$ and $\sigma_{S_{\alpha}^{k_{\text{eff},p}}}$ represent the absolute statistical uncertainties of the sensitivity coefficients obtained from the Monte Carlo calculation, associated with k_{eff} and $k_{\text{eff},p}$, respectively.

The relative uncertainty of β_{eff} due to nuclear-data cross-section uncertainties, denoted as $U_{\beta_{\text{eff}}}$, is the estimated uncertainty of the reactions for each isotope using the Sandwich Rule, illustrated as (Kiedrowski, 2014; MacFarlane et al., 2019):

$$U_{\beta_{\text{eff}}} = \sqrt{\left|[S_{\alpha}^{\beta_{\text{eff}}}]^T[C][S_{\alpha}^{\beta_{\text{eff}}}]\right|} \tag{10}$$

where $[S_{\alpha}^{\beta_{\text{eff}}}]^T$ is the transpose of the vector $[S_{\alpha}^{\beta_{\text{eff}}}]$, showing the sensitivity coefficient in the 44-group model. The [C] is the covariance matrix of the reactions for each isotope in the 44-group model. The ERRORR card of the NJOY code was utilized to estimate the covariance matrix [C] (MacFarlane et al., 2019). Since the covariance matrices are not available in the CENDL-3.2 library, the uncertainties of β_{eff} were calculated exclusively for the ENDF/B-VIII.0, ENDF/B-VIII.1, JEFF-3.3, and JENDL-5 libraries.

4. Results and discussion

4.1. Effective kinetic parameters

Table 3 summarizes the calculated β_{eff} values, comparing the adjoint weighted and prompt k-ratio methods across the major nuclear data libraries ENDF/B-VIII.1, ENDF/B-VIII.0, JENDL-5, JEFF-3.3, and CENDL-3.2. The predicted β_{eff} values span a range from 731 to 769 pcm. Overall, a good agreement between the two computational approaches is observed, yielding discrepancies less than 13 pcm (approximately 1.8%). However, the inter-library variation is more pronounced, reaching a maximum deviation of 38 pcm (5.2%), with JEFF-3.3 yielding the highest β_{eff} values with both methods: 756 pcm with adjoint weighting and 769 pcm with the prompt k-ratio method. These higher values may reflect differences in neutron production data, including delayed-neutron yields and emission spectra, as well as transport data that influence the forward and adjoint neutron distributions. However, the present whole-library comparisons do not isolate these contributions and therefore do not establish that the differences originate solely from the evaluated delayed-neutron group fractions. In contrast, for libraries employing the conventional six-group structure, excellent consistency between the two methods is preserved. Specifically, for the latest ENDF/B-VIII.1 library, the adjoint-weighted method yields 732 pcm compared to 733 pcm from the prompt k-ratio method. This close agreement across different baseline evaluations confirms a robust consensus on the kinetic characteristics of the LEU-fueled DNRR core.

The calculated kinetic parameters derived via the adjoint weighted method show that the β_{eff} results exhibit a narrow spread, ranging from 732 to 756 pcm with a deviation of about 3.3%. The JEFF-3.3 library yields the highest value at 756 pcm, while the minimum is observed with both ENDF/B-VIII.1 and JENDL-5 (732 pcm). The neutron generation time Λ fluctuates between 80.31 and 80.91 μs. The maximum Λ is attained using CENDL-3.2 (80.91 μs), whereas ENDF/B-VIII.0 produces the smallest value of 80.31 μs. For ENDF/B-VIII.0, ENDF/B-VIII.1, and JENDL-5, the values remain close, with a maximum difference of 0.30 μs. Similarly, the prompt neutron lifetime l_p spans a restricted range of 80.45–81.38 μs. The variation for both Λ and l_p remains within about 1.2%, indicating a high consistency among the evaluated nuclear data libraries for the DNRR LEU fueled core. Using the prompt k-ratio method, the calculated β_{eff} values range from 731 to 769 pcm across the data libraries, corresponding to a maximum variation of approximately 5.2%. JEFF-3.3 predicts the highest value (769 pcm), whereas CENDL-3.2 yields the lowest (731 pcm). For ENDF/B-VIII.1, the adjoint weighted and prompt k-ratio methods predict β_{eff} values of 732 and 733 pcm, respectively, differing by only 1 pcm (0.1%).

The delayed neutron group parameters, comprising the fractional yields (β_i), delayed neutron energies, and their respective decay constants (λ_i) and precursor half lives determined via the adjoint weighted method, are detailed in Table 4. For ENDF/B-VIII.0, ENDF/B-VIII.1, JENDL-5, and CENDL-3.2, which employ a six-group delayed neutron representation, the results show that Group 4 is the dominant contributor to the delayed neutron population, with β_4 values in the range of 283–289 pcm. Significant contributions are also observed from Groups 2 and 3, which exhibit β_i values ranging from 127 to 160 pcm. Conversely, the long lived and short lived precursors in Groups 1 and 6 represent the smallest fractions, with Group 6 yielding the minimum contribution, fluctuating between 30 and 49 pcm across the evaluated libraries. The delayed neutron energies are highly consistent among the four libraries, ranging from approximately 0.405 to 0.558 MeV. This hierarchical distribution of β_i is essential for accurately characterizing the reactor response during transient conditions.

The decay constant λ_i characterizes the disintegration rate of delayed neutron precursors; specifically, higher λ_i values denote shorter half lives and accelerated neutron emission. Group 1 consistently exhibits the most stable behavior with the lowest values ($\lambda_1 \approx 0.012$–0.013 s^{-1}), corresponding to the longest lived precursors in the system with half lives ranging from 51.97 to 55.70 s. In contrast, Group 6 demonstrates the most rapid decay kinetics, with λ_6 values ranging from 2.857 to 3.038 s^{-1} and corresponding half lives of approximately 0.23–0.24 s. For the intermediate groups, JENDL-5 reports the highest decay constant for Group 5 (1.143 s^{-1}), corresponding to the shortest half life of 0.61 s within this group, while Group 4 shows a high degree of consistency among the evaluated libraries, maintaining λ_4 in the range of 0.302–0.304 s^{-1} and half lives of approximately 2.28–2.29 s. It is noticed that ENDF/B-VIII.0, ENDF/B-VIII.1, and CENDL-3.2 display highly congruent decay constants and precursor half lives across the majority of groups, with only marginal deviations limited to the short lived Groups 5 and 6. Overall, the precursor half lives span from approximately 55.70 s to 0.23 s for the six-group libraries. These library specific variations in delayed neutron decay characteristics are important for the precise modeling of reactor kinetics during rapid power fluctuations. Owing to the eight-group delayed neutron formulation adopted in JEFF-3.3, the delayed neutron fractions are distributed across an expanded set of groups, with the dominant contribution originating from Group 5 (247 pcm). Furthermore, as summarized in Table 4, the JEFF-3.3 library spans a broader phase space of kinetic parameters than the other libraries, characterized by a wider delayed neutron energy spectrum (0.216–0.621 MeV), a larger range of decay constants (0.012–3.555 s^{-1}), and a wider span of precursor half lives (55.60–0.195 s).

4.2. Sensitivity analysis of β_{eff}

The sensitivity of β_{eff} to various nuclear reaction channels for key isotopes is summarized in Table 5. This evaluation utilizes prominent nuclear data libraries of ENDF/B-VIII.1, ENDF/B-VIII.0, JEFF-3.3, JENDL-5, and CENDL-3.2 to identify the primary drivers of uncertainty in kinetic parameters. Only coefficients with absolute magnitudes exceeding 0.1% (based on the ENDF/B-VIII.0 reference) are reported. The values represent relative sensitivity coefficients (in percentage), quantifying the fractional change in β_{eff} per unit perturbation in specific

Table 4
Delayed neutron group parameters obtained with various nuclear data libraries.

Library	Group (i)	$\beta_{\text{eff},i}$ (pcm)	Energy (MeV)	λ_i (s^{-1})	Half-life (s)
ENDF/B-VIII.0	1	26 ± 1	0.40472 ± 0.00071	0.01334	51.97009
	2	130 ± 1	0.47134 ± 0.00032	0.03273	21.17958
	3	131 ± 1	0.44276 ± 0.00032	0.12080	5.73785
	4	284 ± 2	0.55766 ± 0.00029	0.30304	2.28729
	5	119 ± 1	0.51805 ± 0.00046	0.85063	0.81487
	6	49 ± 1	0.54089 ± 0.00079	2.85682	0.24263
	Total	739 ± 3	–	–	–
ENDF/B-VIII.1	1	25 ± 1	0.40619 ± 0.00072	0.01334	51.96994
	2	134 ± 1	0.47189 ± 0.00032	0.03273	21.17942
	3	127 ± 1	0.44234 ± 0.00032	0.12080	5.73784
	4	283 ± 2	0.55741 ± 0.00029	0.30304	2.28729
	5	115 ± 1	0.51737 ± 0.00046	0.85063	0.81486
	6	48 ± 1	0.53938 ± 0.00079	2.85679	0.24263
	Total	732 ± 3	–	–	–
JENDL-5	1	25 ± 1	0.40516 ± 0.00073	0.01244	55.69727
	2	160 ± 1	0.47159 ± 0.00029	0.03055	22.68688
	3	143 ± 1	0.44258 ± 0.00030	0.11172	6.20434
	4	289 ± 2	0.55717 ± 0.00028	0.30215	2.29401
	5	86 ± 1	0.51734 ± 0.00054	1.14329	0.60628
	6	30 ± 1	0.54147 ± 0.00099	3.03823	0.22814
	Total	732 ± 3	–	–	–
CENDL-3.2	1	26 ± 1	0.40487 ± 0.00071	0.01334	51.97901
	2	131 ± 1	0.47186 ± 0.00032	0.03273	21.17592
	3	128 ± 1	0.44168 ± 0.00032	0.12096	5.7295
	4	283 ± 2	0.55782 ± 0.00029	0.30356	2.28341
	5	118 ± 1	0.51772 ± 0.00046	0.86197	0.80414
	6	48 ± 1	0.54119 ± 0.00079	2.87839	0.24081
	Total	734 ± 3	–	–	–
JEFF-3.3	1	25 ± 1	0.21636 ± 0.00039	0.01247	55.59989
	2	114 ± 1	0.62117 ± 0.00033	0.02829	24.50002
	3	69 ± 1	0.29394 ± 0.00033	0.04252	16.29999
	4	151 ± 1	0.4492 ± 0.00030	0.13304	5.20999
	5	247 ± 2	0.51658 ± 0.00029	0.29247	2.37
	6	70 ± 1	0.48732 ± 0.00062	0.66649	1.04
	7	63 ± 1	0.53909 ± 0.00075	1.63478	0.424
	8	17 ± 1	0.59071 ± 0.00136	3.55460	0.195
	Total	756 ± 3	–	–	–

reaction cross sections. For comparison among the libraries, the results are presented as ratios of E8.1/E8, JF3/E8, J5/E8, and C3/E8, where each library's sensitivity coefficient is normalized against the ENDF/B-VIII.0 baseline. In addition, the statistical uncertainties associated with the sensitivity coefficients are provided to assess the reliability and convergence of the calculated sensitivities.

The delayed neutron fission yield (delayed ν) of U-235 exhibits the highest positive sensitivity in the range of 96%–98% across the evaluated libraries. The inter library sensitivity ratios are E8.1/E8 = 1.00, JF3/E8 = 0.98, J5/E8 = 1.00, and C3/E8 = 1.00. Thermal inelastic and total reactions of light water, characterized by the Thermal Scattering Law (TSL) $S(\alpha,\beta)$, represent the second significant contribution, albeit with substantial discrepancies among the evaluated libraries. Substantial inter-library variations are observed, with sensitivity coefficients of 34.30%, 28.40%, 33.76%, and 15.00% obtained for JEFF-3.3, ENDF/B-VIII.0, ENDF/B-VIII.1, and JENDL-5, respectively. The CENDL-3.2 library lacks data for this reaction channel. The ratio JF3/E8 reaches 1.21, indicating that the TSL in JEFF-3.3 exerts a greater impact on β_{eff} than the ENDF/B-VIII.0 baseline. This variation highlights the importance of TSL modeling in pool type reactors like the DNRR, where the moderation process in light water significantly modulates the neutron importance function.

Beyond the primary fissile isotope data, the TSLs $S(\alpha,\beta)$ of natural carbon and beryllium, together with the scattering reactions of Al-27, represent the subsequent tier of sensitivity contributors. A qualitative disparity is observed in the Al-27 elastic scattering reaction: JENDL-5 predicts a positive sensitivity of 5.88%, contrasting with the negative values reported by ENDF/B-VIII.0 (−9.48%), ENDF/B-VIII.1 (−2.13%), JEFF-3.3 (−13.55%), and CENDL-3.2 (−9.90%). For the total Be $S(\alpha,\beta)$ reaction, the sensitivity coefficient varies from −16.81% in JENDL-5 to 28.04% in JEFF-3.3, whereas the total C-nat $S(\alpha,\beta)$ sensitivity ranges from −5.28% in JEFF-3.3 to 14.82% in JENDL-5. Such discrepancies indicate how structural and moderator materials influence the β_{eff} response. This is further evidenced by the inter library ratios; for Be $S(\alpha,\beta)$ (total), JEFF-3.3 predicts an effect approximately twice as large as ENDF/B-VIII.0 (JF3/E8 = 2.01), while for C-nat $S(\alpha,\beta)$ (total), the influence in JENDL-5 is more than three times greater than that of ENDF/B-VIII.0 (J5/E8 = 3.09). Regarding negative sensitivities, the prompt neutron yield (ν_p) of U-235 exhibits a dominant inverse correlation with β_{eff}, ranging from −98.27% to −95.80%. Within this range, JEFF-3.3 shows a slightly attenuated negative impact (−95.80%) compared to ENDF/B-VIII.0 (−96.90%). Furthermore, while the elastic scattering of H-1 displays a strong negative sensitivity in ENDF/B-VIII.0 (−45.13%), a significant qualitative conflict emerges among the evaluated libraries. ENDF/B-VIII.1 and CENDL-3.2 predict positive contributions of 28.65% and 58.35%, respectively, whereas JEFF-3.3 yields a weak negative value (−3.08%) and JENDL-5 predicts a larger negative sensitivity (−24.01%). These disagreements highlight substantial inconsistencies in the modeling of light water neutron moderation and scattering physics across the evaluated nuclear data libraries.

Fig. 4 illustrates the energy dependent sensitivity profiles of the primary cross sections influencing β_{eff}. The U-235 delayed neutron yield (ν_d) exhibits a dominant positive sensitivity peak within the energy range from 10^{-2} to 10^{-1} eV, corresponding to the thermal region where the major fissions occur in the DNRR core. This sensitivity diminishes to negligible levels at energies exceeding 1.0 eV, confirming that fast fission events have a minimal impact on the overall delayed neutron population. For scattering processes, the Lwtr $S(\alpha,\beta)$ inelastic and total

Table 5
Sensitivity coefficients of β_{eff}, uncertainties of the sensitivity coefficients, and ratios relative to ENDF/B-VIII.0[a].

Isotope	Reaction	ENDF/B-VIII.0		ENDF/B-VIII.1			JEFF-3.3			JENDL-5			CENDL-3.2		
		Sens. (%)	Unc.	Sens. (%)	Unc.	E8.1/E8	Sens. (%)	Unc.	JF3/E8	Sens. (%)	Unc.	J5/E8	Sens. (%)	Unc.	C3/E8
U-235	delayed ν	97.49	0.01	97.74	0.01	1.00	95.74	0.01	0.98	97.97	0.01	1.00	97.71	0.01	1.00
Lwtr S(α,β)	inelastic	28.40	0.34	33.76	0.35	1.19	34.30	0.33	1.21	15.00	0.34	0.53	–	–	–
Lwtr S(α,β)	total	28.40	0.34	33.76	0.35	1.19	34.30	0.33	1.21	15.00	0.34	0.53	–	–	–
Be S(α,β)	elastic	14.83	0.10	−14.64	0.10	−0.99	20.85	0.10	1.41	−18.55	0.11	−1.25	–	–	–
Be S(α,β)	total	13.95	0.12	−16.69	0.12	−1.20	28.04	0.12	2.01	−16.81	0.13	−1.21	–	–	–
C-nat S(α,β)	elastic	11.36	0.09	7.53	0.09	0.66	−0.26	0.09	−0.02	6.25	0.09	0.55	–	–	–
C-nat S(α,β)	total	4.80	0.11	1.52	0.11	0.32	−5.28	0.11	−1.10	14.82	0.11	3.09	–	–	–
U-238	total	2.15	0.04	3.57	0.04	1.66	−2.79	0.04	−1.30	1.12	0.04	0.52	5.64	0.04	2.62
H-1	(n,γ)	1.69	0.01	2.57	0.01	1.52	1.02	0.01	0.60	0.59	0.01	0.35	0.43	0.01	0.25
U-238	elastic	1.56	0.03	2.51	0.03	1.61	−1.21	0.03	−0.78	−0.73	0.03	−0.47	5.20	0.03	3.33
U-238	inelastic	1.55	0.01	−1.16	0.01	−0.75	−2.42	0.01	−1.56	1.34	0.01	0.86	0.65	0.01	0.42
U-238	delayed ν	1.26	0.01	1.27	0.01	1.01	1.32	0.01	1.05	1.36	0.01	1.08	1.38	0.01	1.10
U-235	total ν	0.82	0.07	−0.57	0.07	−0.70	−0.12	0.07	−0.15	−0.18	0.07	−0.22	−0.15	0.07	−0.18
Be-9	(n,γ)	0.75	0.01	0.53	0.01	0.71	0.39	0.01	0.52	0.51	0.01	0.68	0.20	0.01	0.27
U-235	elastic	0.58	0.02	−0.12	0.02	−0.21	0.56	0.02	0.97	−1.21	0.02	−2.09	1.08	0.02	1.86
Be-9	(n,α)	0.57	0.01	0.48	0.01	0.84	0.38	0.01	0.67	0.43	0.01	0.75	0.24	0.01	0.42
Al-27	(n,γ)	0.41	0.01	0.50	0.01	1.22	0.13	0.01	0.32	0.23	0.01	0.56	0.12	0.01	0.29
U-238	(n,γ)	−0.27	0.01	1.65	0.01	−6.11	0.60	0.01	−2.22	0.09	0.01	−0.33	−0.59	0.01	2.19
B-10	elastic	−0.30	0.01	0.38	0.01	−1.27	−0.12	0.01	0.40	0.72	0.01	−2.40	−0.45	0.01	1.50
O-16	inelastic	−0.30	0.01	0.48	0.01	−1.60	−0.55	0.01	1.83	−0.34	0.01	1.13	−0.28	0.01	0.93
Fe-56	total	−0.48	0.01	1.03	0.01	−2.15	0.95	0.01	−1.98	−0.41	0.01	0.85	−1.98	0.01	4.12
U-238	fission	−0.53	0.01	0.58	0.01	−1.09	0.43	0.01	−0.81	0.39	0.01	−0.74	0.36	0.01	−0.68
U-235	(n,γ)	−0.54	0.01	0.56	0.01	−1.04	0.03	0.01	−0.06	−0.52	0.01	0.96	−0.60	0.01	1.11
Fe-56	elastic	−0.56	0.01	0.99	0.01	−1.77	0.92	0.01	−1.64	−0.79	0.01	1.41	−1.80	0.01	3.21
U-238	total ν	−0.70	0.01	0.42	0.01	−0.60	0.26	0.01	−0.37	0.21	0.01	−0.30	0.20	0.01	−0.29
Be-9	elastic	−0.74	0.11	1.42	0.11	−1.92	10.32	0.10	−13.95	10.79	0.11	−14.58	19.67	0.16	−26.58
Al-27	inelastic	−0.83	0.02	−1.16	0.02	1.40	−1.53	0.02	1.84	−0.91	0.02	1.10	−1.21	0.02	1.46
Be S(α,β)	inelastic	−0.87	0.06	−2.05	0.06	2.36	7.18	0.07	−8.25	1.74	0.07	−2.00	–	–	–
U-235	fission	−0.88	0.08	1.92	0.08	−2.18	−0.92	0.08	1.05	−0.97	0.08	1.10	−1.75	0.07	1.99
B-10	(n,γ)	−1.05	0.01	−0.24	0.01	0.23	0.82	0.01	−0.78	0.12	0.01	−0.11	−0.30	0.01	0.29
B-10	total	−1.36	0.01	0.11	0.01	−0.08	−0.16	0.01	0.12	0.69	0.01	−0.51	−0.79	0.01	0.58
U-235	total	−1.50	0.08	3.12	0.08	−2.08	−0.33	0.08	0.22	−1.97	0.08	1.31	−1.03	0.08	0.69
U-238	prompt ν	−1.96	0.01	−0.86	0.01	0.44	−1.06	0.01	0.54	−1.15	0.01	0.59	−1.18	0.01	0.60
Be-9	total	−2.67	0.11	0.58	0.11	−0.22	10.49	0.10	−3.93	6.85	0.11	−2.57	18.15	0.16	−6.80
C-nat	total	−2.97	0.10	14.39	0.10	−4.85	−8.79	0.09	2.96	−10.09	0.10	3.40	−4.66	0.15	1.57
C-nat	elastic	−2.97	0.10	14.28	0.10	−4.81	−8.68	0.09	2.92	−10.03	0.10	3.38	−4.86	0.15	1.64
O-16	elastic	−4.02	0.12	13.41	0.12	−3.34	−0.53	0.12	0.13	12.75	0.12	−3.17	4.81	0.12	−1.20
O-16	total	−4.07	0.12	14.00	0.12	−3.44	−1.02	0.12	0.25	12.63	0.12	−3.10	4.63	0.12	−1.14
C-nat S(α,β)	inelastic	−6.56	0.06	−6.01	0.06	0.92	−5.02	0.06	0.77	8.57	0.06	−1.31	–	–	–
Al-27	elastic	−9.48	0.10	−2.13	0.10	0.22	−13.55	0.10	1.43	5.88	0.11	−0.62	−9.90	0.10	1.04
Al-27	total	−9.81	0.11	−2.71	0.11	0.28	−14.93	0.10	1.52	5.24	0.11	−0.53	−10.91	0.10	1.11
H-1	total	−43.40	0.24	31.23	0.23	−0.72	−2.06	0.23	0.05	−23.34	0.23	0.54	58.76	0.36	−1.35
H-1	elastic	−45.13	0.24	28.65	0.23	−0.63	−3.08	0.23	0.07	−24.01	0.23	0.53	58.35	0.36	−1.29
U-235	prompt ν	−96.90	0.07	−98.27	0.07	1.01	−95.80	0.07	0.99	−98.18	0.07	1.01	−97.87	0.07	1.01

[a] Absolute value of ENDF/B-VIII.0 > 0.1%.

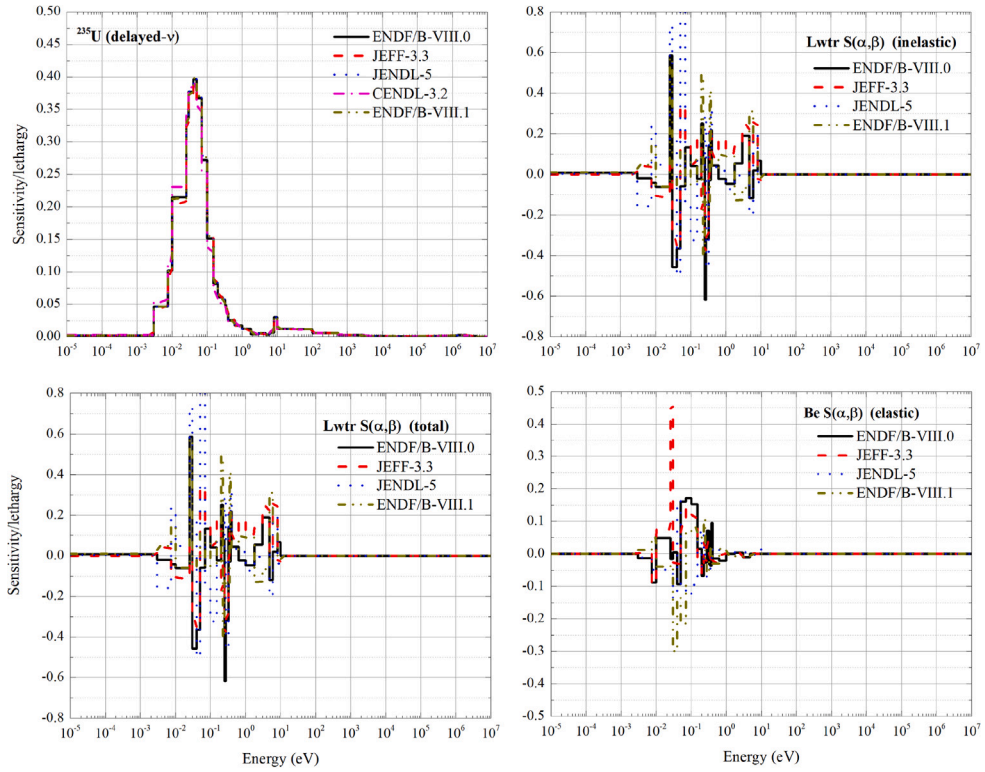


Fig. 4. Energy dependent sensitivities of the β_{eff} of U-235, Lwtr S(α, β), and Be S(α, β).

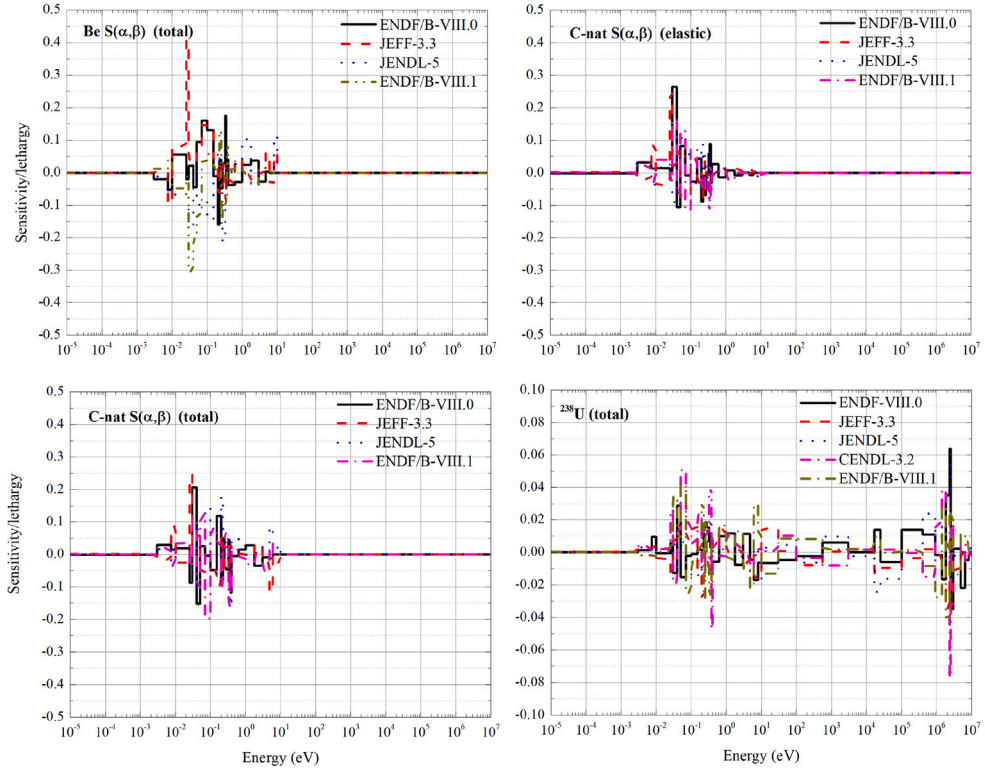


Fig. 5. Energy dependent sensitivities of the β_{eff} of Be S(α, β), C-nat S(α, β), and U-238.

TSLs, together with the Be $S(\alpha, \beta)$ elastic scattering kernel, exhibit pronounced sensitivity fluctuations within the thermal energy range of approximately 10^{-2}–10^{1} eV, highlighting the important role of neutron thermalization. Since TSL data are defined only in the thermal energy region, the corresponding sensitivities vanish outside this range. The same behavior is observed for all TSL based reactions. These profiles indicate that the kinetic behavior is most susceptible to nuclear data uncertainties within the thermal and epithermal energy ranges.

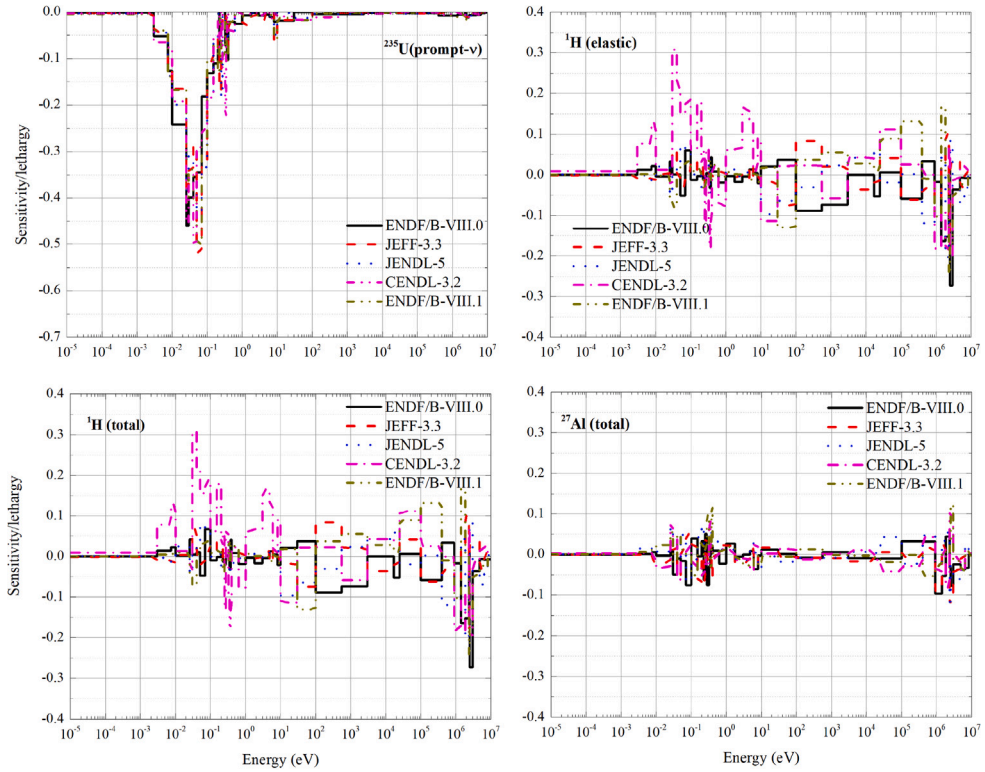


Fig. 6. Energy dependent sensitivities of the β_{eff} of U-235, H-1, and Al-27.

Table 6
Comparison of reaction-wise relative uncertainty contributions to β_{eff} for different nuclear data libraries.

Isotope	Reaction	ENDF/B-VIII.0 (pcm)	ENDF/B-VIII.1 (pcm)	E8.1/E8	JEFF-3.3 (pcm)	JF3/E8	JENDL-5 (pcm)	J5/E8
Total	–	923.3[a]	1033.3	1.12	913.3	0.99	357.6	0.39
Al-27	elastic	607.5	588.2	0.97	861.5	1.42	–	–
B-10	(n,γ)	430.8	124.5	0.29	182.0	0.42	71.7	0.17
Be-9	elastic	372.6	186.3	0.50	–	–	–	–
H-1	elastic	235.9	197.9	0.84	22.3	0.09	97.3	0.41
Al-27	inelastic	203.3	239.6	1.18	75.8	0.37	–	–
O-16	(n,γ)	119.2	57.1	0.48	0.7	0.01	57.9	0.49
Be-9	(n,γ)	115.7	96.2	0.83	–	–	–	–
U-238	inelastic	79.6	44.0	0.55	167.8	2.11	174.6	2.19
U-238	elastic	75.9	117.7	1.55	60.6	0.80	202.7	2.67
Be-9	$n,2n$	71.5	134.8	1.89	–	–	–	–
O-16	inelastic	69.7	111.7	1.60	55.1	0.79	53.3	0.76
O-16	elastic	60.7	708.1	11.66	31.0	0.51	62.2	1.02
C-nat	elastic	55.9	78.7	1.41	46.0	0.82	–	–
H-1	(n,γ)	35.0	53.2	1.52	26.1	0.75	12.2	0.35
U-235	fission	29.4	19.4	0.66	43.2	1.47	19.0	0.64
Be-9	(n,α)	27.6	22.7	0.82	–	–	–	–
U-235	inelastic	25.1	24.5	0.97	5.7	0.23	74.2	2.96
U-235	elastic	22.3	40.3	1.80	75.6	3.39	115.8	5.18
B-10	elastic	22.3	22.4	1.00	20.5	0.92	12.9	0.58
Fe-56	elastic	16.9	16.9	1.00	58.8	3.48	102.8	6.09
O-16	(n,α)	15.4	6.8	0.44	1.4	0.09	8.1	0.52
Fe-56	inelastic	12.3	14.4	1.17	9.5	0.78	22.9	1.87
U-234	elastic	10.6	18.6	1.75	18.8	1.77	15.2	1.43
C-nat	inelastic	9.0	13.0	1.44	22.2	2.46	–	–
B-10	(n,α)	8.9	2.1	0.24	0.3	0.04	3.3	0.38
U-234	inelastic	8.2	7.7	0.94	13.4	1.64	8.6	1.05
Al-27	(n,γ)	7.9	8.9	1.13	32.4	4.12	–	–
U-238	fission	6.7	7.2	1.08	7.9	1.18	7.0	1.04
U-238	(n,γ)	6.4	23.0	3.59	12.0	1.86	8.9	1.39
U-235	(n,γ)	4.8	4.3	0.90	7.8	1.62	4.8	1.01
U-234	(n,γ)	3.8	2.6	0.67	0.2	0.06	6.9	1.81
Fe-56	(n,γ)	2.4	8.6	3.58	0.6	0.24	19.3	8.04
C-nat	(n,γ)	1.8	2.4	1.31	0.1	0.07	–	–

[a] Relative uncertainties are reported in pcm (1 pcm = 0.001%).

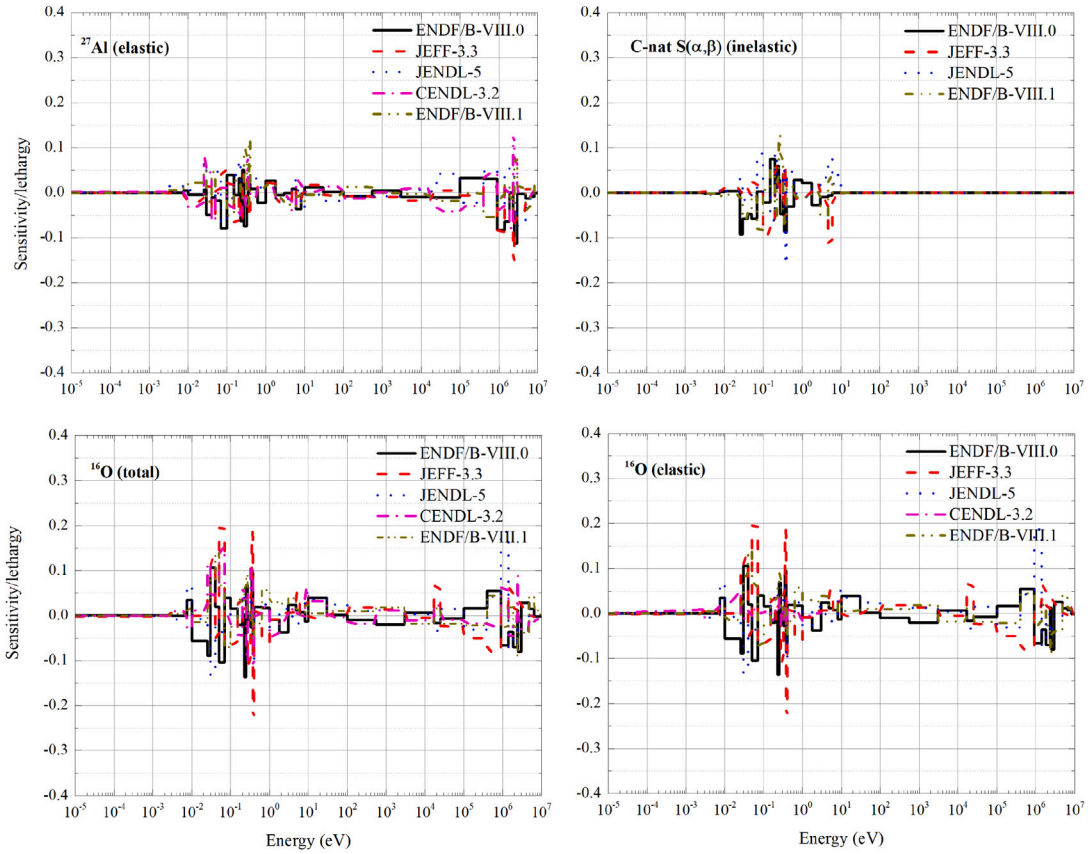


Fig. 7. Energy dependent sensitivities of the β_{eff} of Al-27, C-nat S(α, β), and O-16.

The energy dependent sensitivity profiles of Be $S(\alpha, \beta)$ (total), C-nat $S(\alpha, \beta)$ (elastic and total), and U-238 (total) are shown in Fig. 5. The sensitivity coefficients of the U-238 total reaction span from the thermal to the fast neutron energy ranges. In contrast, the sensitivities of Be $S(\alpha, \beta)$ (total) and C-nat $S(\alpha, \beta)$ (elastic and total) are localized primarily in the 10^{-2}–10^{1} eV. These profiles indicate that while U-238 interactions affect β_{eff} over a broad portion of the neutron energy spectrum, the effects of graphite and beryllium thermal scattering are strongly coupled to neutron thermalization processes.

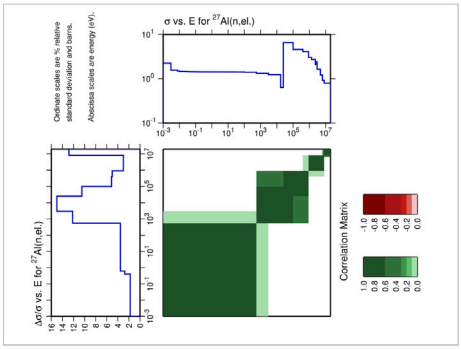
The sensitivity profiles for U-235 (ν_p), H-1 (total and elastic), and Al-27 (total) are depicted in Fig. 6. A profound negative sensitivity is observed for the U-235 prompt neutron yield, specifically within the thermal range below 10^{1} eV, with a prominent peak between 10^{-2} and 10^{-1} eV. This inverse relationship highlights that enhanced prompt neutron production from U-235 effectively dilutes the delayed neutron fraction, thereby reducing β_{eff}. In contrast, the H-1 reactions exhibit relatively small sensitivities in the 2.10^{-3}–10^{1} eV range, while more pronounced sensitivity variations appear in the fast neutron spectrum (10^{3}–10^{7} eV). Meanwhile, the Al-27 total reaction maintains relatively low magnitude sensitivity oscillations over a broad energy range, from the thermal region to the fast neutron domain.

In Fig. 7, the energy dependent sensitivity profiles of Al-27 (elastic), C-nat $S(\alpha, \beta)$ (inelastic), and O-16 (elastic and total) are presented. The sensitivity coefficients of Al-27 elastic scattering and O-16 elastic and total scattering extend from the thermal to the fast neutron energy regions. In contrast, the sensitivity of the C-nat $S(\alpha, \beta)$ inelastic kernel is concentrated in the 10^{-1}–10^{0} eV.

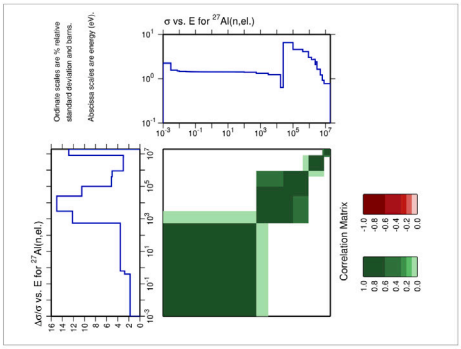
Nuclear reaction sensitivity coefficients quantify the first-order local response of β_{eff} to perturbations in evaluated nuclear data parameters. Within a linear approximation, inter-library variations in the integral β_{eff} depend on both these sensitivity profiles and the underlying cross-section discrepancies. Because sensitivity coefficients exhibit alternating positive and negative values across different reaction channels and energy regimes, localized disparities partially compensate upon energy integration. Furthermore, cross-section variations generally shift k_{eff} and $k_{\text{eff,p}}$ in a coherent direction, thereby constraining their ratio and preserving the integral β_{eff}.

4.3. Relative uncertainty analysis of β_{eff}

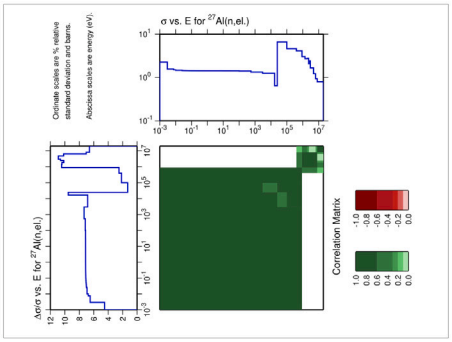
Table 6 summarizes the β_{eff} relative uncertainties originating from nuclear reaction cross section variations across four libraries: ENDF/B-VIII.0, ENDF/B-VIII.1, JEFF-3.3, and JENDL-5. To facilitate comparative analysis, the relative ratios E8.1/E8, JF3/E8, and J5/E8 are provided, utilizing ENDF/B-VIII.0 as the baseline. The aggregate relative uncertainties for these libraries are 923.3, 1033.3, 913.3, and 357.6 pcm, respectively. Compared to the ENDF/B-VIII.0 results, the relative uncertainties derived from JEFF-3.3 and JENDL-5 are lower by approximately 1.1% and 61.3%, respectively, while the ENDF/B-VIII.1 result is higher by approximately 11.9%. A critical factor influencing these results is the absence of covariance data for certain isotopes in JEFF-3.3 and JENDL-5, specifically for Al-27, Be-9, and C-12. Consequently, relative uncertainties associated with capture, $(n, 2n)$, (n, α), elastic, and inelastic scattering for these isotopes remain unquantified in those libraries. This lack of comprehensive covariance information significantly contributes to the reduced total relative uncertainty values reported for JEFF-3.3 and JENDL-5. Specifically, several reactions that contribute significantly to the relative uncertainty in the ENDF/B-VIII.0 library are unavailable in JEFF-3.3 and/or JENDL-5. These include Be-9 elastic scattering (372.6 pcm), Be-9 (n, γ) (115.7 pcm), Be-9 $(n, 2n)$ (71.5 pcm), and C-nat elastic scattering (55.9 pcm), highlighting their substantial impact on the total relative uncertainty budget. Assuming that the relative uncertainties for reactions involving the missing isotopes in JEFF-3.3 and JENDL-5 are taken from ENDF/B-VIII.0, the total relative



(a) ENDF/B-VIII.0



(b) ENDF/B-VIII.1



(c) JEFF-3.3

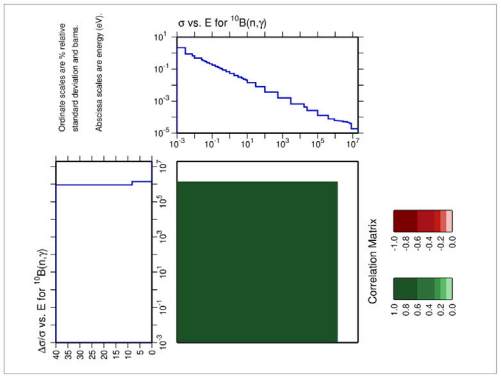
Fig. 8. Covariance data plot for Al-27 (n,elastic).

uncertainties associated with the libraries would be 996.1 and 811.3 pcm, respectively. Under this assumption, JENDL-5 would still yield the smallest total relative uncertainty among the evaluated libraries.

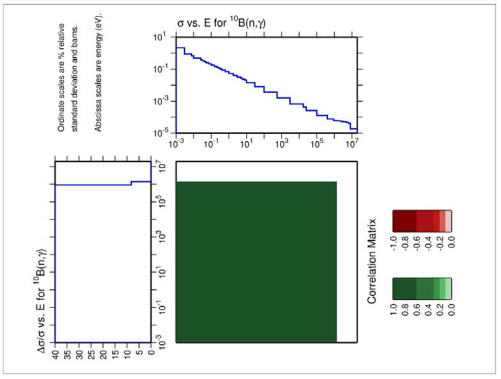
The relative uncertainty budget of β_{eff} is dominated by the elastic scattering reactions of Al-27, Be-9, and H-1, as well as the B-10 (n,γ) reaction. According to the ENDF/B-VIII.0 library, these reactions contribute 607.5, 372.6, 235.9, and 430.8 pcm to the total relative uncertainty, respectively. A notable discrepancy exists in the elastic scattering of Al-27, which contributes 607.5 pcm in ENDF/B-VIII.0, compared with 588.2 pcm in ENDF/B-VIII.1 and 861.5 pcm in JEFF-3.3, while remaining unquantified in JENDL-5 due to missing covariance data. Similarly, the B-10 (n,γ) reaction accounts for 430.8 pcm in ENDF/B-VIII.0, 124.5 pcm in ENDF/B-VIII.1, 182.0 pcm in JEFF-3.3, and 71.7 pcm in JENDL-5, demonstrating considerable library to library variation. The Be-9 elastic scattering reaction contributes 372.6 pcm in ENDF/B-VIII.0 and 186.3 pcm in ENDF/B-VIII.1, but it lacks corresponding entries in JEFF-3.3 and JENDL-5. Significant inconsistencies are also observed in the H-1 elastic scattering channel, with relative uncertainty estimates of 235.9 pcm (ENDF/B-VIII.0), 197.9 pcm (ENDF/B-VIII.1), 22.3 pcm (JEFF-3.3), and 97.3 pcm (JENDL-5). The observed differences in isotope wise uncertainties among the evaluated nuclear data libraries are primarily governed by variations in sensitivity coefficients (see Figs. 4–7) and the corresponding energy dependent covariance data (see Figs. 8–12). In particular, the differences for H-1 are visually corroborated in Figs. 6 and 11, which depict the energy dependent sensitivity profiles and corresponding cross section uncertainties of H-1 elastic scattering. These disparities in the covariance files underscore the non negligible impact of light element data on the accuracy of the kinetic parameters.

In ENDF/B-VIII.1, the relative uncertainty for O-16 elastic scattering is notably higher (708.1 pcm) than that derived from the other libraries because of the combined effect of its energy dependent sensitivity coefficients and the corresponding covariance data, as shown in Figs. 7 and 12. In addition, the Al-27 elastic scattering reaction in JEFF-3.3 has a substantially higher relative uncertainty of 861.5 pcm. While fission and inelastic scattering reactions, particularly of U-235 and U-238, contribute to the total relative uncertainty budget, their impact is secondary compared to that of structural and moderator materials. This is also due to lower uncertainty of uranium nuclear data. Other isotopic contributions arise from the elastic, inelastic, and capture cross sections of B-10, O-16, natural carbon, and Fe-56. Fig. 9 compares the uncertainty profiles for B-10 capture cross sections, showing that while the covariance data across ENDF/B-VIII.0, ENDF/B-VIII.1, JEFF-3.3, and JENDL-5 are broadly consistent at approximately 40%, the resulting integrated uncertainty remains dependent. These discrepancies confirm that variations in covariance matrices are the primary drivers of the observed fluctuations in the quantified uncertainty of β_{eff}. In summary, the scattering and capture properties of Al-27, Be-9, H-1, B-10, and O-16 collectively exert a profound influence on the β_{eff} relative uncertainty. This significance is linked to their role as essential constituents of the DNRR core, where they dictate the neutron moderation and neutron absorption characteristics.

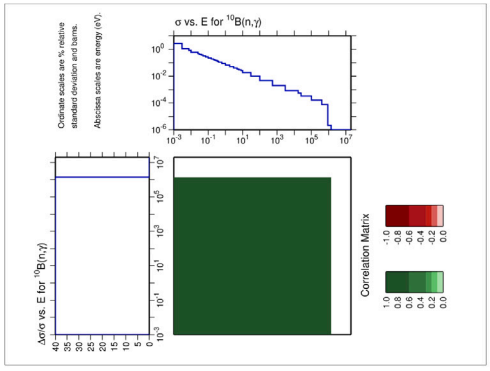
Crucially, the variation of β_{eff} (731–769 pcm) across the investigated data libraries directly impacts the definition of the operational safety envelope for the DNRR. A lower predicted β_{eff} (such as CENDL-3.2 at 731 pcm) implies a more conservative and restricted safety margin before the onset of prompt criticality. This is important for the setting of safety rod trip thresholds during accidental reactivity insertions. Furthermore, in a practical transient scenario, the uncertainties propagate directly into the kinetics equations, affecting in the predicted peak fuel temperature and power pulse. By quantifying this uncertainty, the present study provides important input for the development of a conservative Best Estimate Plus Uncertainty (BEPU) safety assessment framework for the DNRR. In particular, the cross-section-induced



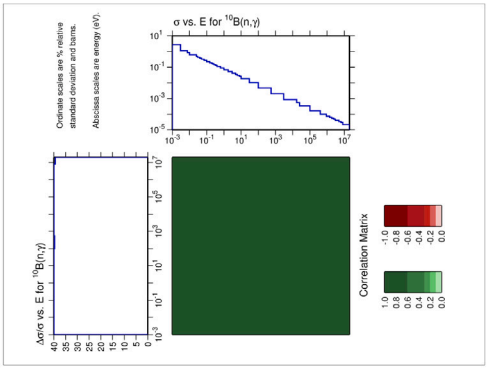
(a) ENDF/B-VIII.0



(b) ENDF/B-VIII.1

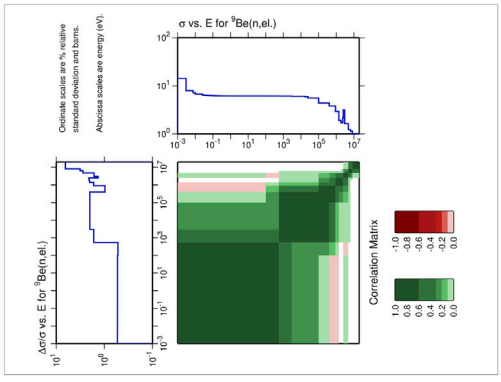


(c) JEFF-3.3

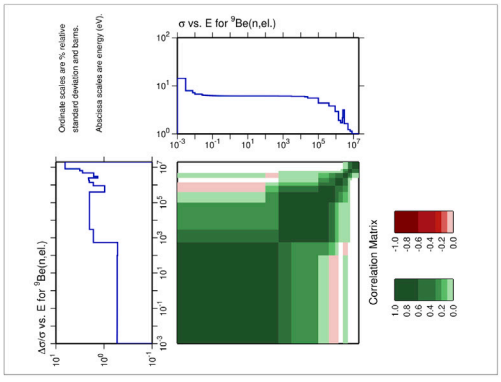


(d) JENDL-5

Fig. 9. Covariance data plot for B-10 (n, γ).

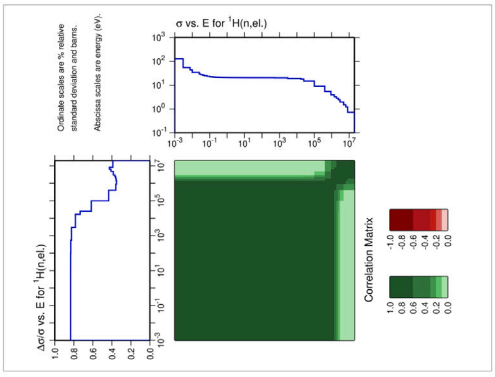


(a) ENDF/B-VIII.0

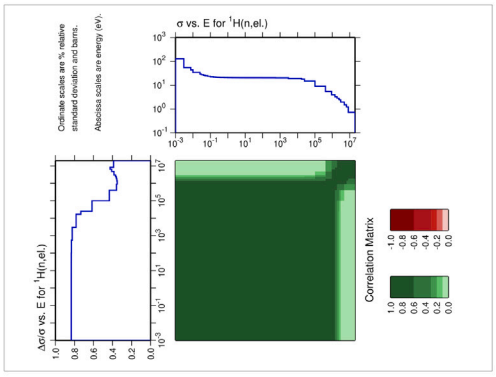


(b) ENDF/B-VIII.1

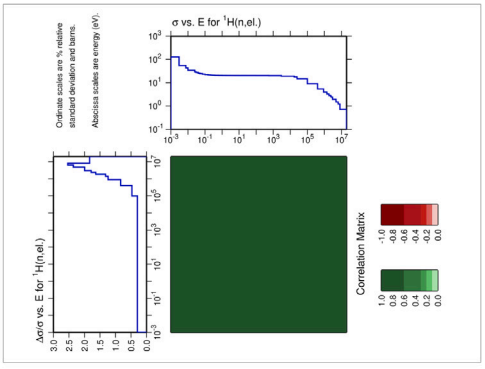
Fig. 10. Covariance data plot for Be-9 (n, elastic).



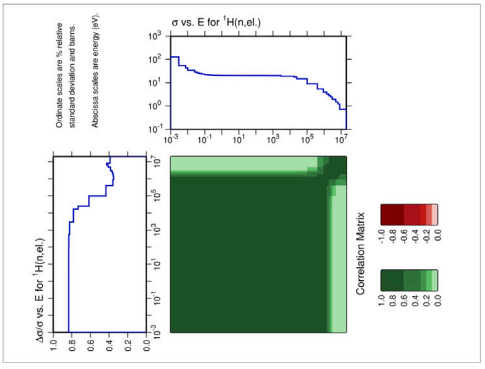
(a) ENDF/B-VIII.0



(b) ENDF/B-VIII.1



(c) JEFF-3.3



(d) JENDL-5

Fig. 11. Covariance data plot for H-1 (n, elastic).

uncertainty represents one of the important nuclear-data uncertainty components that should be considered within a comprehensive BEPU analysis.

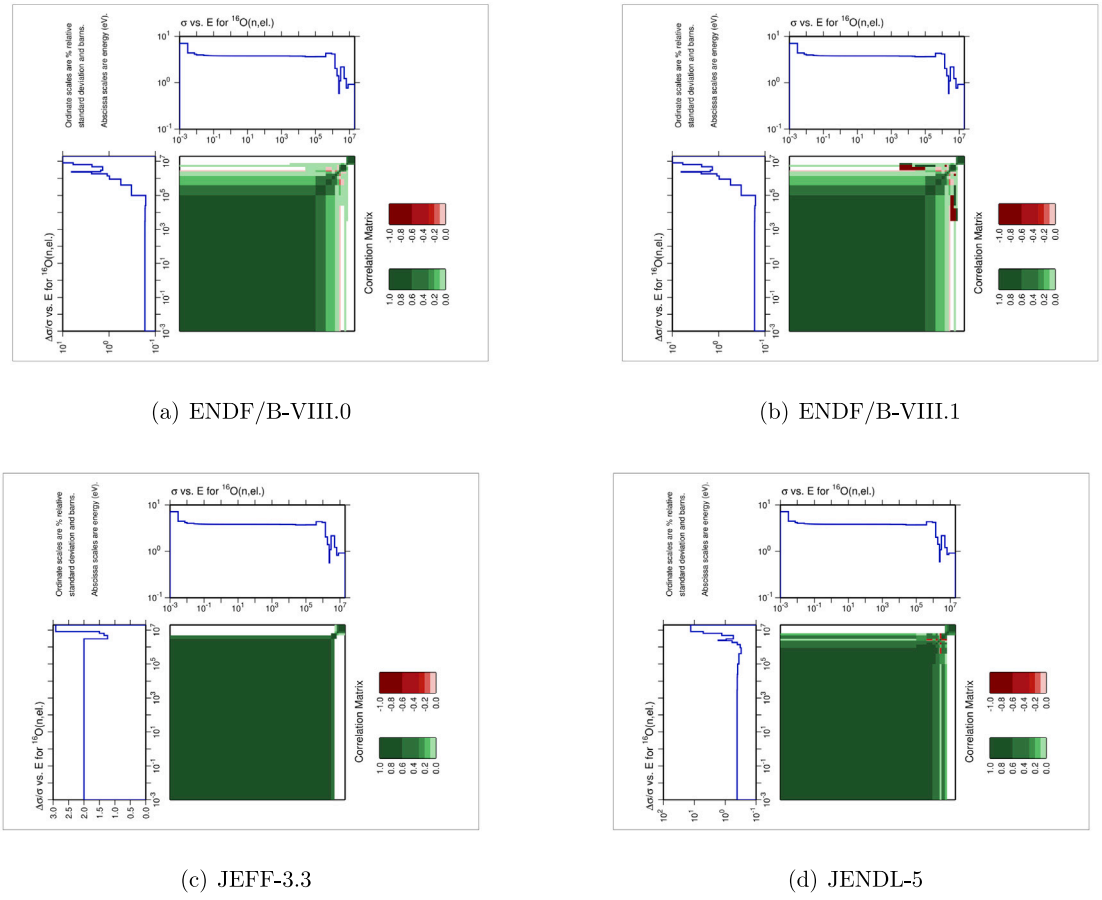
It must be emphasized that the present uncertainty quantification focuses primarily on neutron-induced reaction cross sections. Although the sensitivity of β_{eff} to the average number of prompt and delayed neutrons released per fission event (ν_p and ν_d of U-235) is substantial, these components were not directly propagated in the current calculations due to the absence of complete, mutually consistent covariance matrices for fission neutron multiplicities across all investigated libraries. Consequently, the total uncertainties reported in this work represent the nuclear data-induced uncertainty originating specifically from reaction cross sections. Furthermore, evaluated covariance matrices for the TSL data for light water and beryllium are not available in the public release of the investigated data libraries. Therefore, despite the high sensitivity coefficients observed, the uncertainty propagation for the TSL component could not be performed.

5. Conclusions

A comprehensive evaluation of the kinetic parameters and the associated β_{eff} uncertainties for the DNRR LEU fueled core has been conducted using the MCNP6.3 code and the latest evaluated nuclear data libraries, including ENDF/B-VIII.0, ENDF/B-VIII.1, JEFF-3.3, JENDL-5, and CENDL-3.2. The calculated β_{eff} values derived via the adjoint weighted and prompt k-ratio methods show good agreement among the libraries, ranging from 731 to 769 pcm. The discrepancies between the adjoint weighted and prompt k-ratio methods remained below 1.8%, whereas the inter library variation of the adjoint weighted β_{eff} values was approximately 3.3%. For the reference ENDF/B-VIII.0 library, the kinetic characteristics were quantified with high statistical accuracy, yielding the β_{eff} of 739 pcm, together with the Λ and the l_p of 80.31 μs and 80.45 μs, respectively.

Relative uncertainty analysis revealed that the total β_{eff} relative uncertainty is primarily governed by elastic scattering reactions. The elastic scattering of Al-27 was identified as a dominant contributor, accounting for approximately 65.8% (ENDF/B-VIII.0), 56.9% (ENDF/B-VIII.1), and 94.3% (JEFF-3.3) of the corresponding total relative uncertainties. Depending on the evaluated library, reaction channels contributing notably to the uncertainty threshold include B-10 (n,γ), Be-9 elastic, H-1 elastic, O-16 elastic, and U-238 elastic and inelastic scattering. Variations in the β_{eff} relative uncertainty of reaction cross sections for isotopes across libraries mainly arise from differences in energy dependent sensitivity profiles and nuclear covariance data. Uncertainties associated with the delayed-neutron group fractions β_i and the prompt and delayed fission neutron yields should be incorporated once the required covariance data become available in the evaluated nuclear data libraries.

The results provide a quantitative framework for evaluating nuclear data uncertainty propagation in the DNRR calculations, and identify the dominant reactions that contribute to the uncertainty budget of kinetic parameters. The importance of comprehensive covariance data for uncertainty quantification is also indicated. Although the absence of covariance information does not necessarily reflect the quality of the underlying evaluated nuclear data, it limits the ability to estimate uncertainty propagation and may lead to an incomplete assessment of uncertainties relevant to reactor safety margin analyses. In terms of practical application, the substantial variations observed in kinetic parameters emphasize the necessity of accounting for library dependent discrepancies in reactor safety analyses. The identification of the primary uncertainty drivers provides reactor operators and regulators with



(a) ENDF/B-VIII.0

(b) ENDF/B-VIII.1

(c) JEFF-3.3

(d) JENDL-5

Fig. 12. Covariance data plot for O-16 (n, elastic).

the exact reaction channels required to define conservative safety envelopes during accidental reactivity insertions. Ultimately, integrating these uncertainties into transient modeling establishes a solid foundation toward a standardized best estimate plus uncertainty (BEPU) framework for the DNRR.

CRediT authorship contribution statement

Duc-Tu Dau: Writing – review & editing, Writing – original draft, Methodology, Formal analysis. **Nhi-Dien Nguyen:** Writing – review & editing, Formal analysis. **Giang T.T. Phan:** Writing – review & editing, Formal analysis. **Huu-Tiep Nguyen:** Writing – review & editing, Formal analysis. **Peng Hong Liem:** Writing – review & editing, Formal analysis. **Hoai-Nam Tran:** Writing – review & editing, Writing – original draft, Supervision, Methodology, Formal analysis, Conceptualization.

Declaration of competing interest

The authors declare that they have no known competing financial interests or personal relationships that could have appeared to influence the work reported in this paper.

Acknowledgment

This research was funded by National Foundation for Science and Technology Development (NAFOSTED), Vietnam under grant 103.04-2023.116.

Data availability

The data that has been used is confidential.

References

Akyurek, T., Shoaib, S., Usman, S., 2021. Delayed fast neutron as an indicator of burn-up for nuclear fuel elements. Nucl. Eng. Technol. 53, 3127–3132. http://dx.doi.org/10.1016/j.net.2021.04.013.

Arkani, M., Hassanzadeh, M., Khakshournia, S., 2016. Calculation of six-group importance weighted delayed neutron fractions and prompt neutron lifetime of MTR research reactors based on Monte Carlo method. Prog. Nucl. Energy 88, 352–363. http://dx.doi.org/10.1016/j.pnucene.2015.12.005.

Bretscher, M., 1997. Evaluation of reactor kinetic parameters without the need for perturbation codes. In: Proceedings of the International Meeting on Reduced Enrichment for Research and Test Reactors. Jackson Hole, WY, USA.

Cacuci, D.G., Ionescu-Bujor, M., Navon, I.M., 2005. Sensitivity and Uncertainty Analysis: Applications to Large-Scale Systems, vol. II, CRC Press Taylor & Francis, Boca Raton, FL 33487-2742.

Chu, T.N., Phan, G.T.T., Tran, L.Q.L., Bui, T.H., Do, Q.B., Dau, D.T., Nguyen, K.C., Nguyen, N.D., Nguyen, H.T., Hoang, V.K., Vu, T.M., Tran, H.N., 2024. Sensitivity and uncertainty analysis of the first core of the DNRR using MCNP6 and new nuclear data libraries. Nucl. Eng. Des. 419, 112986. http://dx.doi.org/10.1016/j.nucengdes.2024.112986.

Dau, D.T., Nguyen, N.D., Huynh, T.N., Pham, Q.H., Nguyen, K.C., Chu, T.N., Hoang, V.K., Phan, G.T., Nguyen, H.T., Vu, T.M., Tran, H.N., 2025a. Criticality and sensitivity/uncertainty analysis of the DNRR with LEU fuel using MCNP6.3 and the latest data libraries. Nucl. Eng. Des. 442, 114182. http://dx.doi.org/10.1016/j.nucengdes.2025.114182.

Dau, D.T., Nguyen, N.D., Nguyen, H.T., Chu, T.N., Tran, H.N., 2025b. Sensitivity of kinetic parameters to operation parameters of the dalat nuclear research reactor with LEU fuel. J. Phys.: Conf. Ser. 3040, 012020. http://dx.doi.org/10.1088/1742-6596/3040/1/012020.

Dau, D.T., Nguyen, N.D., Nguyen, K.C., Pham, Q.H., Chu, T.N., Hoang, V.K., Phan, G.T., Tran, H.N., 2025c. Kinetic parameters of the dalat nuclear research reactor with LEU fuel using MCNP6 and JENDL-5 library. Nucl. Technol. Radiat. Prot. 40, 1–9. http://dx.doi.org/10.2298/NTRP2501001D.

Do, Q.B., Phan, G.T.T., Nguyen, K.C., Ngo, Q.H., Tran, H.N., 2019. Criticality and rod worth analysis of the DNRR research reactor using the SRAC and MCNP5 codes. Nucl. Eng. Des. 343, 197–209. http://dx.doi.org/10.1016/j.nucengdes.2019.01.011.

Hanson, L.A., Diamond, D., 2012. Calculation of Kinetics Parameters for the NBSR. Technical Report, Brookhaven National Laboratory (BNL), Upton, NY, United States, http://dx.doi.org/10.2172/1043393.

Hanson, L.A., Ludewig, H., Diamond, D.J., 2006. Calculation of the prompt neutron lifetime in the NBSR. Nucl. Sci. Eng. 153, 26–32. http://dx.doi.org/10.13182/NSE06-4.

Hendricks, J., et al., 2006. MCNPX, VERSION 2.6.B. Technical Report LA-UR-06-3248, Los Alamos National Laboratory.

Hosseini, S., Vosoughi, N., Ghofrani, M., Gharib, M., 2010. Calculation, measurement and sensitivity analysis of kinetic parameters of tehran research reactor. Ann. Nucl. Energy 37, 463–470. http://dx.doi.org/10.1016/j.anucene.2010.01.018.

Keepin, G., 1965. Physics of Nuclear Kinetics. Addison-Wesley, Reading, MA.

Khan, M., Sarker, M., Islam, S., 2013. Analysis of kinetic parameters of 3MW TRIGA mark-II research reactor using the SRAC2006 code system. Ann. Nucl. Energy 60, 181–186. http://dx.doi.org/10.1016/j.anucene.2013.05.009.

Kiedrowski, B.C., 2014. Methodology for Sensitivity and Uncertainty-Based Criticality Safety Validation. Technical Report, Vols. LA-UR-14-23202.

Kiedrowski, B.C., Brown, F.B., 2013. Adjoint-based k-eigenvalue sensitivity coefficients to nuclear data using continuous-energy monte carlo. Nucl. Sci. Eng. 174, 227–244. http://dx.doi.org/10.13182/NSE12-46.

Kodeli, I.A., 2013. Sensitivity and uncertainty in the effective delayed neutron fraction β_{eff}. Nucl. Instrum. Methods Phys. Res. Sect. A: Accel. Spectrometers, Detect. Assoc. Equip. 715, 70–78. http://dx.doi.org/10.1016/j.nima.2013.03.020.

Kulesza, J.A., Adams, T.R., Armstrong, J.C., Bolding, S.R., Brown, F.B., Bull, J.S., Burke, T.P., Clark, A.R., Forster, III, R.A., Giron, J.F., Grieve, T.S., Josey, C.J., Martz, R.L., McKinney, G.W., Pearson, E.J., Rising, M.E., Solomon, Jr., C.J., Swaminarayan, S., Trahan, T.J., Wilson, S.C., Zukaitis, A.J., 2022. MCNP® Code Version 6.3.0 Theory & User Manual. Technical Report LA-UR-22-30006, Rev. 1, Los Alamos National Laboratory, Los Alamos, NM, USA, http://dx.doi.org/10.2172/1889957.

Liem, P.H., Zuhair, Hartanto, D., 2019. Sensitivity and uncertainty analysis on the first core criticality of the RSG GAS multipurpose research reactor. Prog. Nucl. Energy 114, 46–60. http://dx.doi.org/10.1016/j.pnucene.2019.03.001.

MacFarlane, R.E., Muir, D.W., Boicourt, R.M., Kahler, A.C., Conlin, J.L., Haeck, W., 2019. The NJOY Nuclear Data Processing System. Los Alamos, NM, United States.

Makhloul, M., Boukhal, H., Chakir, E., El Bardouni, T., Lahdour, M., Kaddour, M., Ahmed, A., Arectout, A., El Yaakoubi, H., 2022. Sensitivity and uncertainty quantification of neutronic integral data in the TRIGA Mark II research reactor. Nucl. Eng. Technol. 54, 523–531. http://dx.doi.org/10.1016/j.net.2021.08.003.

Meulekamp, R.K., van der Marck, S.C., 2006. Calculating the effective delayed neutron fraction with monte carlo. Nucl. Sci. Eng. 152, 142–148. http://dx.doi.org/10.13182/NSE03-107.

Mweetwa, B., Ampomah-Amoako, E., Akaho, E., Odoi, C., 2018. Prediction of neutronic and kinetic parameters of ghana research reactor 1 (GHARR-1) after 19 years of operation using Monte Carlo-n particle (MCNP) code. World J. Nucl. Sci. Technol. 8, 160–175. http://dx.doi.org/10.4236/wjnst.2018.84014.

Nagaya, Y., 2015. Calculation of reactor kinetics parameters with monte carlo differential operator sampling. Ann. Nucl. Energy 82, 226–229. http://dx.doi.org/10.1016/j.anucene.2014.08.064.

Nguyen, N.D. (Editor), 2003. Safety Analysis Report for the Dalat Nuclear Research Reactor. Technical Report, Nuclear Research Institute, Vietnam Atomic Energy Commission.

Nguyen, N.D., Luong, B.V., Le, V.V., Duong, V.D., Nguyen, X.H., Phan, N.S., Cao, D.V., 2014. Results of operation and utilization of the dalat nuclear research reactor. Nucl. Sci. Technol. 4, 1–9.

Nguyen, N.D., et al., 2012. Safety Analysis Report for the Dalat Nuclear Research Reactor. Technical Report, Nuclear Research Institute, Vietnam Atomic Energy Institute.

OECD, 2017. International Handbook of Evaluated Reactor Physics Benchmark Experiments. OECD Nuclear Energy Agency.

Phan, G., Tran, H.N., Nguyen, K.C., Tran, V.P., Hoang, V.K., Ha, P.N.V., Kiet, H.A.T., 2017. Comparative analysis of the Dalat nuclear research reactor with HEU fuel using SRAC and MCNP5. Sci. Technol. Nucl. Install. 2017, 10. http://dx.doi.org/10.1155/2017/2615409, Article ID 2615409.

Pinem, S., Liem, P.H., Luthfi, W., Surbakti, T., Hartanto, D., 2024. Evaluation of kinetic parameters RSG-GAS reactor equilibrium silicide core using continuous-energy Monte Carlo serpent 2 code. Nucl. Sci. Eng. 198, 1935–1949. http://dx.doi.org/10.1080/00295639.2023.2284433.

Romero-Barrientos, J., Damián, J.M., Molina, F., Zambra, M., Aguilera, P., López-Usquiano, F., Parra, B., Ruiz, A., 2022. Calculation of kinetic parameters β_{eff} and Λ with modified open source Monte Carlo code OpenMC(TD). Nucl. Eng. Technol. 54, 811–816. http://dx.doi.org/10.1016/j.net.2021.09.020.

Talamo, A., Gohar, Y., 2010. Deterministic and Monte Carlo Modeling and Analyses of YALINA-Thermal Subcritical Assembly. Technical Report ANL-NE-10/17, Argonne National Laboratory, URL https://www.osti.gov/bridge.

Tran, V.P., Nguyen, K.C., Hartanto, D., Tran, H.N., Tran, V.T., Hoang, V.K., Ha, P.N.V., 2021. Development of a PARCS/Serpent model for neutronics analysis of the dalat nuclear research reactor. Nucl. Sci. Tech. 32, 15. http://dx.doi.org/10.1007/s41365-021-00855-5.

Zhong, Z., Talamo, A., Gohar, Y., 2013. Monte carlo and deterministic computational methods for the calculation of the effective delayed neutron fraction. Comput. Phys. Comm. 184, 1660–1665. http://dx.doi.org/10.1016/j.cpc.2013.02.009.